14. K. J. Friston, C. D. Frith, R. S. J. Frackowiak, *Hum. Brain Mapp.* **1**, 69 (1993).
15. M. L. Furey *et al.*, *Proc. Natl. Acad. Sci. U.S.A.* **94**, 6512 (1997).
16. D. J. Veltman, S. A. Rombouts, R. J. Dolan, *Neuroimage* **18**, 247 (2003).
17. K. Christoff *et al.*, *Neuroimage* **14**, 1136 (2001).
18. I. H. Jenkins, D. J. Brooks, P. D. Nixon, R. S. Frackowiak, R. E. Passingham, *J. Neurosci.* **14**, 3775 (1994).
19. E. Koechlin, A. Danek, Y. Burnod, J. Grafman, *Neuron* **35**, 371 (2002).
20. R. L. Buckner, W. Koutstaal, *Proc. Natl. Acad. Sci. U.S.A.* **95**, 891 (1998).
21. J. B. Rowe, I. Toni, O. Josephs, R. S. Frackowiak, R. E. Passingham, *Science* **288**, 1656 (2000).
22. A. Dove, S. Pollmann, T. Schubert, C. J. Wiggins, D. Y. von Cramon, *Brain Res. Cogn. Brain Res.* **9**, 103 (2000).
23. Y. Nagahama *et al.*, *Cereb. Cortex* **11**, 85 (2001).
24. K. Sakai, R. E. Passingham, *Nature Neurosci.* **6**, 75 (2003).
25. E. Koechlin, G. Basso, P. Pietrini, S. Panzer, J. Grafman, *Nature* **399**, 148 (1999).
26. E. Koechlin, G. Corrado, P. Pietrini, J. Grafman, *Proc. Natl. Acad. Sci. U.S.A.* **97**, 7651 (2000).
27. P. S. Goldman-Rakic, in *Handbook of Physiology, The Nervous System*, F. Plum, V. Moutcastle, Eds. (American Physiological Society, Bethesda, MD, 1987), vol. 5, pp. 373–417.
28. T. Shallice, *From Neuropsychology to Mental Structure* (Cambridge Univ. Press, New York, 1988).
29. A. Baddeley, S. Della Sala, *Philos. Trans. R. Soc. London Ser. B* **351**, 1397 (1996).
30. G. T. Fechner, *Elemente der Psychophysik* (Breitkopf and Härtel, Leipzig, Germany, 1860).
31. K. H. Norwich, W. Wong, *Percept. Psychophys.* **59**, 929 (1997).

32. We thank S. Dehaene, J. Grafman, and E. Guigon for helpful discussions and the Service Hospitalier Frédéric Joliot (Orsay, France) for MRI facilities. Supported by the French Ministry of Research (Action Concertée Incitative grant no. 22-2002-350) and the Institut Fédératif de Recherche d'Imagerie Neurofonctionelle (IFR49).

Supporting Online Material

www.sciencemag.org/cgi/content/full/302/5648/1181/DC1
Materials and Methods
SOM Text
Figs. S1 and S2
Table S1
References

27 June 2003; accepted 30 September 2003

REPORTS

Persistence of Memory in Drop Breakup: The Breakdown of Universality

Pankaj Doshi,[1]* Itai Cohen,[2] Wendy W. Zhang,[3]† Michael Siegel,[4] Peter Howell,[5] Osman A. Basaran,[1] Sidney R. Nagel[3]

A low-viscosity drop breaking apart inside a viscous fluid is encountered when air bubbles, entrained in thick syrup or honey, rise and break apart. Experiments, simulations, and theory show that the breakup under conditions in which the interior viscosity can be neglected produces an exceptional form of singularity. In contrast to previous studies of drop breakup, universality is violated so that the final shape at breakup retains an imprint of the initial and boundary conditions. A finite interior viscosity, no matter how small, cuts off this form of singularity and produces an unexpectedly long and slender thread. If exterior viscosity is large enough, however, the cutoff does not occur because the minimum drop radius reaches subatomic dimensions first.

Underlying one of the common occurrences of daily life, the breakup of a liquid drop, is a rich and beautiful phenomenon. As a drop divides, the neck connecting the different masses of fluid necessarily becomes arbitrarily thin with a curvature that grows without bound until molecular scales are reached. Because surface tension gives rise to a pressure proportional to the curvature, this pressure also diverges. Similar singularities, in which a physical quantity effectively diverges, occur in many different realms, ranging from the subatomic-nuclear fission (*1*) to the celestial-star formation (*2*). The ubiquity, simplicity, and accessibility of drop breakup makes it ideal for studying divergent dynamical behavior that occurs elsewhere in nature.

Near such a singularity, the dynamics are normally governed by the proximity to the singularity, and the dynamics become universal so that all memory of initial and boundary conditions is lost. In such cases, the breakup becomes scale-invariant; after appropriate rescaling, drop shapes near the breakup can be superimposed at different times onto a single form, depending on only a few material parameters (*3*–*6*).

Here, we report an important exception to this class of behavior: the breakup of a zero-viscosity drop inside an extremely viscous exterior fluid produces an unexpected, nonuniversal form of singularity, in which the memory of the initial conditions persists throughout the breakup process. Axial structure imposed at the outset on large length scales remains as the thin neck collapses. The unusual character of this breakup suggests a novel and controllable method for producing submicrometer structures.

Because all classical fluids have a finite viscosity, it is important to understand the nature of the singularity when the interior viscosity is very small but nonzero. If the interior viscosity is sufficiently small, as it is for an air bubble in thick syrup, the zero-viscosity drop breakup dynamics persist down to the atomic scales. However, if the interior viscosity is large enough, or the exterior viscosity small enough, the singularity will be cut off. In this case, the large-scale shape of the drop assumes an unexpected appearance. The smooth profile is transformed into a long and thin thread, which can be less than 1 μm thick. The drop and surrounding fluid in our experiment were chosen to display the zero-viscosity drop breakup dynamics, which remember initial and boundary conditions, and the subsequent destruction of the dynamics by the effect of a finite interior viscosity.

Figure 1 shows a water drop with an interior fluid viscosity $\mu_{int} = 0.01$ poise (1 poise = 1 g cm^{-1} s^{-1}) as it drips through silicone oil (polydimethylsiloxane) with an exterior fluid viscosity of $\mu_{ext} = 120$ poise. The drop shape near the minimum forms a quadratic profile that remains smooth and symmetric about the minimum as the neck collapses radially (Fig. 1, A to C). This quadratic regime, with constant axial curvature, persists until the neck thins to a radius of about 100 μm, at which point the thinning of the neck slows dramatically. The slowing begins at the minimum and propagates axially so that a thin thread is formed connecting the two conical regions of the drop (Fig. 1, D and E). Finally, the drop breaks at the two ends of the thread.

In both experiments and simulations, we investigated the dynamics of the quadratic breakup regime (Fig. 1, A to C) by measuring the radius of the drop profile $h(z, t)$ as a function of z, the axial position measured from the min-

[1]School of Chemical Engineering, Purdue University, West Lafayette, IN 47907, USA. [2]Physics and Division of Engineering and Applied Sciences, Harvard University, Cambridge, MA 02138, USA. [3]The Physics Department and the James Franck Institute, University of Chicago, Chicago, IL 60637, USA. [4]Department of Mathematical Sciences, New Jersey Institute of Technology, Newark, NJ 07102, USA. [5]Mathematical Institute, 24–29 Saint Giles', Oxford OX 13LB, UK.

*Present address: Department of Chemical Engineering, Massachusetts Institute of Technology, Cambridge, MA 02139, USA.
†To whom correspondence should be addressed. E-mail: wzhang@uchicago.edu

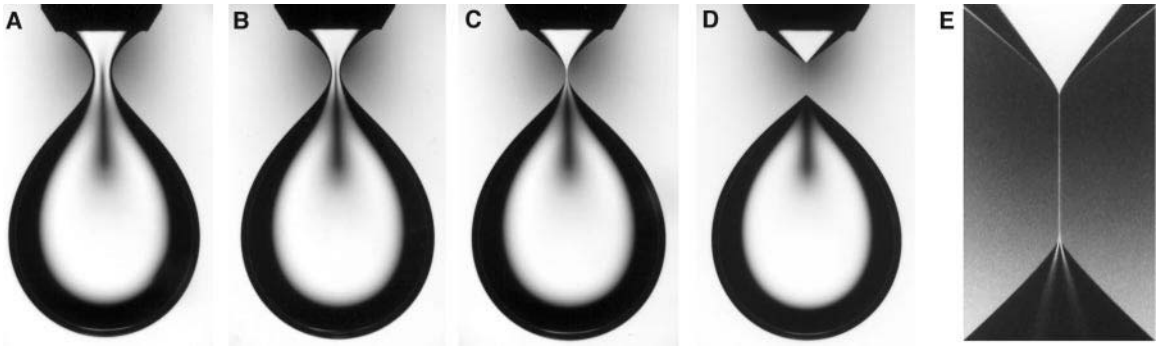

Fig. 1. A 0.01-poise water drop dripping through 120-poise silicone oil. The inner diameter of the nozzle is 4.7 mm. (**A** to **C**) Quadratic breakup regime. The quadratic profile near the minimum collapses radially. (**D**) Effect of drop viscosity alters the drop shape from a quadratic with one minimum to a long and thin thread. (**E**) A close-up of the 8-μm radius and 2-mm-long thread bridging two conical regions of the drop.

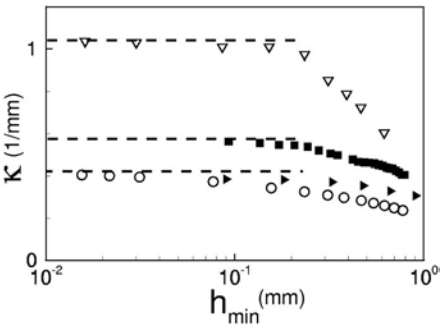

Fig. 2. Axial curvature at the minimum κ versus h_{min} for two dripping drop experiments (solid symbols) with slightly different inner nozzle diameters (4.7 mm for solid triangles and 6.2 mm for solid squares) and two cylinder breakup simulations (open symbols) with significantly different initial perturbation wavelengths (3.9 cm for open triangles and 2.2 cm for open circles, with average cylinder radius fixed at 6.2 mm). The experimental measurement errors are on the order of the symbol size, and the simulation errors are smaller than the symbol size. Different initial or boundary conditions produced different asymptotic axial curvatures.

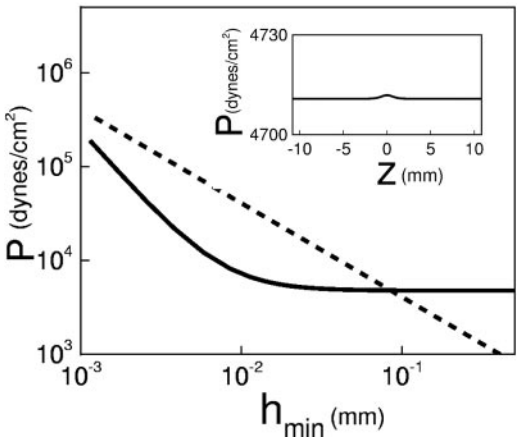

Fig. 3. Maximum interior pressure (solid line) and surface-tension pressure (dashed line) from simulation of water in viscous silicone oil breakup, with $\mu_{int}/\mu_{ext} = 10^{-4}$. The pressure first remains constant, then diverges as h_{min}^{-2}. The cutoff radius h_{cutoff} is about 10^{-3} mm from the scaling argument. The inset shows the interior-pressure profile along the drop centerline when $h_{min} = 0.1$ mm. The pressure varies by less than 0.02% over the entire drop. To show this slight variation, the pressure axis is restricted to a narrow range from 4700 to 4730 dynes cm^{-2}.

imum value of radius h, and time t. We used the finite-element method to simulate the breakup by solving the Navier-Stokes equations for the interior and exterior flows. Instead of a dripping drop, the simulation tracks how a sinusoidal perturbation on a liquid cylinder causes the cylinder to break up. The algorithm has successfully captured the breakup dynamics for drops of varying viscosities dripping through air, including the successive creation of satellite droplets (*7*, *8*). Figure 2 shows a plot of κ, the axial curvature at the minimum, versus the minimum radius, h_{min}, for two experiments with slightly different nozzle diameters and two simulations with substantially different initial perturbations. In all four cases, the axial curvature curves approach constant values at small h_{min}. Thus, near its minimum, the neck shape is collapsing with a uniform radial velocity. Unexpectedly, different initial conditions and boundary conditions lead to different asymptotic axial curvatures. This suggests that the quadratic regime corresponds to a breakup that does not result in a universal profile but instead remembers the quadratic profile near the minimum posed by the initial and boundary conditions.

To investigate this unusual behavior, we examined the simulation and found the leading-order force balance to be between surface tension and exterior viscous stress. This force balance gives rise to a collapse velocity proportional to γ/μ_{ext}, which is independent of absolute length scale and which results in h_{min} decreasing linearly with time, in both experiments and simulations. We next examined the pressure profile from the simulation and found that the interior pressure is virtually uniform in space, varying by less than 0.02% over the entire drop (Fig. 3, inset). The absence of a pressure gradient indicates that the interior flow, and the interior inertia, is negligible. The drop interior thus behaves as if it were static.

Previous studies have shown that drops break only as fast as the surface-tension effects can squeeze interior fluid out of the thinning neck (*3*, *4*, *9*). As a consequence, the breakup obeys a local volume-flux conservation law. In the regime just discussed, this conservation law is irrelevant to the dynamics. The drop breaks only as fast as the surface-tension effect can induce the exterior flow to collapse inward. Interior flow effects are negligible. The local volume-flux conservation law that was previously relevant for breakup is transformed into a condition of uniform interior pressure.

The idea described above is captured quantitatively by a simple model of breakup when $\mu_{int} = 0$. Because the quadratic profile near the minimum is long and slender, the breakup dynamics are well approximated by the collapse of a hollow cylinder inside a viscous fluid. We modeled the exterior velocity field as the result of a line of point sinks situated along the drop centerline. The strength of the sinks is determined by requiring that, at the surface, the velocity of the exterior fluid equals the collapse velocity of the drop. This allows us to derive an expression for the exterior viscous stress on the drop surface. Balancing the exterior viscous stress against surface-tension pressure and interior pressure yields the evolution equation for the drop profile

$$\frac{2\,\mu_{ext}}{h(z,t)}\frac{\partial h(z,t)}{\partial t} - P(t) + \frac{\gamma}{h(z,t)} = 0 \quad (1)$$

The first term corresponds to the exterior viscous stress, the second term corresponds to the interior pressure, and the third term corresponds to the surface-tension pressure. The reference pressure is the exterior pressure far from the breaking drop. The steady-state version of Eq. 1 was first derived by Buckmaster (*10*). The interior pressure $P(t)$ is related to the drop profile by means of an integral that constrains the drop volume to be constant over time (*11*). Thus the drop-shape evolution is in general nonlinear, even with this simple model. However, a drastic simplification occurs near breakup because $P(t)$ is bounded and becomes progressively unimportant compared with the exterior viscous stress and the surface-tension pressure, both of which diverge. Moreover, the divergences in

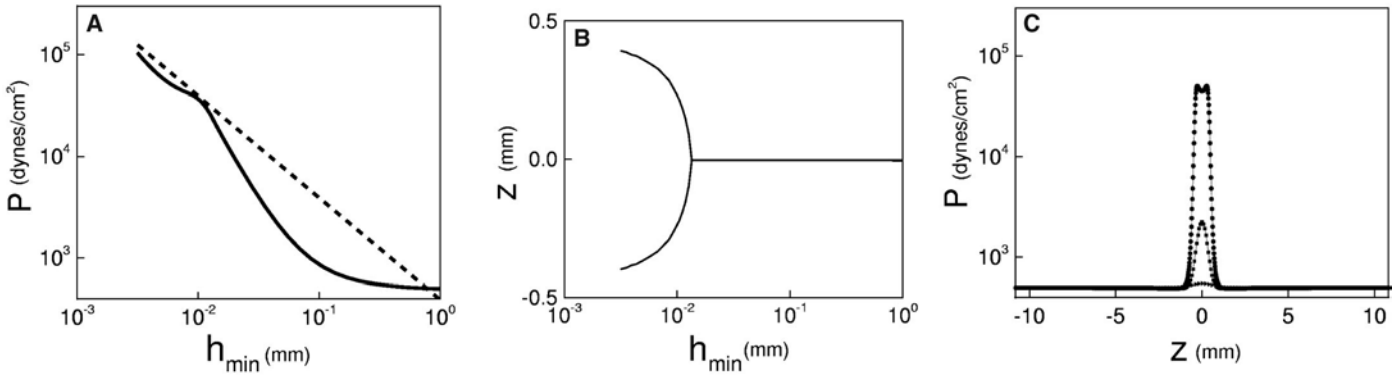

Fig. 4. Simulation of breakup for $\mu_{int}/\mu_{ext} = 10^{-3}$. (**A**) Maximum interior pressure (solid line) and surface-tension pressure (dashed line). The trend is similar to Fig. 3 except that the interior pressure becomes comparable with surface-tension pressure at $h_{cutoff} \approx 10^{-2}$ mm. (**B**) Axial location of the minimum, *z*, versus minimum radius, h_{min}. The single minimum splits into two minima, which move apart as $\sqrt{(h_{cutoff} - h_{min})}$. (**C**) Interior centerline pressure profiles when h_{min} equals 0.1, 0.01, and 0.002 mm. The initial spatially uniform pressure develops a pronounced peak as interior viscous dissipation becomes significant. After the minimum splits into two, the pressure develops a double peak.

the two stresses cancel in an unusually simple way, resulting in the profile near the minimum collapsing with a radial velocity $\gamma/2\mu_{ext}$, which is independent of axial position. The generic initial condition, which is a quadratic shape near the minimum, is preserved until breakup.

This model enables us to draw several important conclusions about the breakup dynamics. Because points on the surface near the minimum move radially inward with the same velocity, the axial length scale does not vary as h_{min} decreases to 0. The breakup is not self-similar. This is also why the axial curvature at the minimum κ, which is inversely proportional to the typical axial length scale z_0, remains constant as h_{min} decreases to 0 (*12*) (Fig. 2). Because the breakup region does not change in the axial direction, the profile retains an imprint of the imposed initial and the boundary conditions. Thus, the final breakup profile is nonuniversal (Fig. 2).

In contrast, previously studied examples of drop breakup produce nonlinear dynamics, so that the drop shape is invariant within a contracting region characterized by a decreasing radial length scale h_{min} and a decreasing axial length scale z_0. Because this region contracts to a point at breakup, the drop shape outside the region is linked together discontinuously, creating a kink instead of the smooth quadratic profile observed here. The scale-invariant dynamics erase all memory of initial and boundary conditions.

We now consider how a nonzero interior viscosity can cut off this quadratic regime. The retarding effect of viscous dissipation associated with the interior fluid having to squeeze out of a thinning neck, initially negligible, becomes significant close to the breakup. We can estimate the interior viscous dissipation during the quadratic breakup regime. The size of the interior velocity U_{int} is set by the local volume-flux conservation $\pi h_{min}^2 U_{int} \approx z_0 2\pi h_{min}(dh_{min}/dt)$, which requires that the local thinning of the thread dh_{min}/dt be balanced by the axial flow out of the local region. The resultant estimate for U_{int} shows that the interior viscous stress $\mu_{int}U_{int}/h_{min}$ increases as h_{min}^{-2}, which is more rapid than the h_{min}^{-1} divergence of the surface-tension pressure. We can check this argument by looking at the simulations for the perturbed cylinder. They show that the maximum interior pressure, which has one contribution from global volume conservation and another from interior viscous dissipation, increases as h_{min}^{-2} and becomes comparable with surface-tension pressure as h_{min} decreases to h_{cutoff}, the cutoff radius (Fig. 3). Above h_{cutoff}, our simulations show that interior viscous dissipation is negligibly small, consistent with the model presented above. Below h_{cutoff}, the breakup is expected to slow significantly, because the viscous resistance has a large contribution from the interior flow in addition to the exterior flow. The scaling argument also predicts that h_{cutoff} is smaller than the initial drop radius by a factor of about μ_{int}/μ_{ext}. For a drop that is 1 cm in radius and μ_{int}/μ_{ext} values that are 10^{-8} or less, the quadratic breakup regime persists down to a minimum radius of a few angstroms, by which point the continuum approximation breaks down. At such small values of μ_{int}/μ_{ext}, as is the case for an air bubble in thick syrup, the breakup is entirely in the asymptotic $\mu_{int} = 0$ regime, for which the quadratic breakup analysis is valid throughout.

For larger values of μ_{int}/μ_{ext}, the finite viscosity of the drop brings out a qualitative change in the large-scale structure of the drop profile (Fig. 1, D and E). Unfortunately, this change, which occurs around h_{cutoff}, lies outside of the simulation range for $\mu_{int}/\mu_{ext} = 10^{-4}$. To view this regime, we performed the simulation at $\mu_{int}/\mu_{ext} = 10^{-3}$, which has a larger h_{cutoff}. Figure 4A shows the behavior for the larger μ_{int}/μ_{ext} and clearly demonstrates that the interior pressure does not increase above the surface-tension pressure. As the breakup enters the new regime, the two minima move apart as $\sqrt{(h_{cutoff} - h_{min})}$ (Fig. 4B). Figure 4C shows the development of a double peak in the interior-pressure profile. The results in Fig. 4, B and C, are consistent with the idea that the initially quadratic profile is slowed down and blunted by the interior viscous stresses, which can no longer be neglected below h_{cutoff}. The values of h_{cutoff} in the cylinder breakup simulations are smaller than those observed in the falling drop experiment, most likely because of the difference in the boundary and initial condition and because of additional stresses created by the falling drop. However, in contrast to h_{cutoff}, the dimensionless aspect ratio for the thin thread in the experiment is within experimental error of that obtained from the scaling argument. Finally, the drop breaks under a balance of interior and exterior viscous stresses and surface tension, a regime previously shown to give rise to universal breakup profiles in the form of two connected cones (*4*, *13*–*16*).

Both aspects of the breakup process—the reproduction of the initial profile on smaller ones during the quadratic regime and the subsequent formation of a long, thin thread—are controllable. The large exterior viscosity also damps out noise from the environment, unlike other breakup regimes (*9*). Moreover, the evolution of structure is slow. A 1-cm drop of 0.2-poise fluid in a surrounding fluid of 2×10^5 poise breaks at the rate of 3 $\mu m\ s^{-1}$ and creates a thread with a radius of about 100 nm. A thin solid thread could thus be manufactured by adding a prepolymer (which does not change the viscosity or the rheology) to the interior fluid, and then rapidly photopolymerizing it during the appropriate stage of breakup. If we assume that bulk polymerization rates (*17*) are relevant for the geometry of a thin thread, then the slow rate of collapse should allow ample time for the thread to solidify. This is being attempted for encapsulation (*18*). For coating technologies in which air entrainment in viscous fluids is an issue (*19*–*21*), our study suggests that the entrained-bubble size distribution can be tuned by increasing the exterior viscosity. Increasing the exterior viscosity so that the breakup dynamics lie entirely in the quadratic

regime also eliminates satellite drops. This makes it possible to manufacture monodisperse gas bubbles in a viscous flow, analogous to techniques being developed to manufacture such bubbles in inertial flows (*22*). The viscous flow regime is relevant for the processing of foods, pharmaceuticals, and metal foams.

In conclusion, we observed nonuniversal, linear dynamics accompanying the formation of a smooth singularity in the breakup of a water drop in viscous silicone oil. This is the asymptotic regime for small enough values of μ_{int}/μ_{ext}, so that the interior viscosity can be neglected throughout the breakup process. For larger μ_{int}/μ_{ext}, the interior viscosity becomes important before atomic dimensions are reached. This produces a long and thin thread. The linear dynamics associated with the formation of a singularity demonstrate that there are two ways for the formation of a singularity to simplify dynamics. In the generic case, the singularity dynamics become scale-invariant, confined to a region that shrinks in all dimensions, thereby erasing all memory of boundary and initial conditions. In the case studied here, the dynamics near the singularity are characterized by an axially uniform radial collapse, so that the axial length scale remains constant, thereby making it possible for memory of the initial and boundary conditions to persist.

References and Notes

1. N. Bohr, *Nature* **143**, 330 (1939).
2. S. Chandrasekhar, *An Introduction to the Study of Stellar Structure* (Dover, New York, 1967).
3. J. Eggers, *Rev. Mod. Phys.* **69**, 865 (1997).
4. I. Cohen, S. R. Nagel, *Phys. Fluids* **13**, 3533 (2001).
5. R. E. Goldstein, A. I. Pesci, M. J. Shelley, *Phys. Rev. Lett.* **70**, 3043 (1993).
6. R. Almgren, A. L. Bertozzi, M. P. Brenner, *Phys. Fluids* **8**, 1356 (1996).
7. A. U. Chen, P. K. Notz, O. A. Basaran, *Phys. Rev. Lett.* **88**, 4501 (2002).
8. P. K. Notz, A. U. Chen, O. A. Basaran, *Phys. Fluids* **13**, 549 (2001).
9. X. D. Shi, M. P. Brenner, S. R. Nagel, *Science* **265**, 219 (1994).
10. J. D. Buckmaster, *J. Fluid Mech.* **55**, 385 (1972).
11. More precisely, it can be shown that the interior pressure $P(t)$ is given by $P(t) = \pi(\gamma/a^3) \int_{\text{drop length}} h(z, t)dz$, where a is a typical radial length scale, chosen to make the dimensionless drop volume equal to 1.
12. For nonlinear breakup dynamics, the axial curvature at the mininum κ is related to the typical axial length scale z_0 by means of $\kappa \propto h_{min}/z_0^2$. Here, $\kappa \propto 1/z_0$ because the linear breakup dynamics have no z dependence.
13. I. Cohen, M. P. Brenner, J. Eggers, S. R. Nagel, *Phys. Rev. Lett.* **83**, 1146 (1999).
14. W. W. Zhang, J. R. Lister, *Phys. Rev. Lett.* **83**, 1151 (1999).
15. A. Sierou, J. R. Lister, *J. Fluid Mech.*, in press.
16. Though we observe an approximately 100° cone for the large drop just before the breakup, the limited range of length scale over which we observe the conical profile makes it difficult to determine whether the observed cone is an asymptotic structure.
17. G. Odian, *Principles of Polymerization* (Wiley-Interscience, New York, 1991).
18. I. Cohen, H. Li, J. L. Hougland, M. Mrksich, S. R. Nagel, *Science* **292**, 265 (2001).
19. P. G. Simpkins, V. J. Kuck, *Nature* **403**, 641 (2000).
20. J. Eggers, *Phys. Rev. Lett.* **86**, 4290 (2001).
21. E. Lorenceau, F. Restagno, D. Quere, *Phys. Rev. Lett.* **91**, 184501 (2003).
22. A. M. Gañán-Calvo, J. M. Gordillo, *Phys. Rev. Lett.* **87**, 274501 (2001).

23. We thank D. Gifford for early experimental contribution to this project, and M. P. Brenner, J. Eggers, J. R. Lister, and H. A. Stone for useful discussions. Supported by the Basic Energy Sciences program of the U.S. Department of Energy (P.D. and O.A.B.); NSF grant DMR-0089081 (to I.C. and S.R.N.); NSF grant DMS-0104350 (to M.S.); and an NSF Mathematical Sciences Postdoctoral Research Fellowship (DMS-0102033), NSF grant DMR-0094569 (to L.P. Kadanoff), and the Materials Research Science and Engineering Center of NSF (to W.W.Z.).

16 July 2003; accepted 7 October 2003

A Superconducting Reversible Rectifier That Controls the Motion of Magnetic Flux Quanta

J. E. Villegas,[1] Sergey Savel'ev,[2] Franco Nori,[2,3] E. M. Gonzalez,[1] J. V. Anguita,[4] R. García,[4] J. L. Vicent[1]*

We fabricated a device that controls the motion of flux quanta in a niobium superconducting film grown on an array of nanoscale triangular pinning potentials. The controllable rectification of the vortex motion is due to the asymmetry of the fabricated magnetic pinning centers. The reversal in the direction of the vortex flow is explained by the interaction between the vortices trapped on the magnetic nanostructures and the interstitial vortices. The applied magnetic field and input current strength can tune both the polarity and magnitude of the rectified vortex flow. Our ratchet system is explained and modeled theoretically, taking the interactions between particles into consideration.

Motor proteins play a key role in the transport of materials at the cellular level (*1–3*). These biological motors are anisotropic devices that, driven by nonequilibrium fluctuations, bias the motion of particles, and which are inspiring a new generation of solid-state devices (*3–5*) that can open avenues for controlling the motion of electrons, colloidal particles, and magnetic flux quanta. Here we consider superconducting devices with anisotropic pinning, where the dc transport of magnetic flux quanta may be driven by an ac or unbiased current. Control of vortex motion with asymmetric pinning can be useful for applications in superconductivity, including field-dependent reversible vortex diodes and the removal of unwanted trapped flux from devices. Several different ways of using asymmetric pinning in superconductors to control vortex motion have been recently proposed (*6–13*). However, experiments in this area (*14*, *15*) have been difficult to control.

Earlier work on vortex dynamics in superconducting films (*16*) with regular arrays of defects (*17*, *18*), using either nonmagnetic (*19–22*) or magnetic (*23–30*) pinning traps, have explored a plethora of physical effects, including matching effects with ordered submicron magnetic defects, interstitial vortices, random versus periodic pinning, and channeling effects in the vortex lattice motion. Now that the field of vortex dynamics on periodic pinning potentials is sufficiently understood, we are in a position to take the next step of manipulating and controlling the motion of magnetic flux quanta. Preliminary numerical studies (*10*, *11*) of vortex dynamics on arrays of triangular pinning potentials have found that rectified vortex motion should occur when the system is ac-driven.

We fabricated arrays of submicron Ni triangles with electron beam lithography (*29*) on Si(100) substrates and then deposited a 100-nm-thick Nb film by dc magnetron sputtering. Several samples were fabricated with different sizes and positions of the triangles (Fig. 1A and fig. S1). For transport measurements, a cross-shaped bridge was optically lithographed and ion-etched on the Nb films (Fig. 1B, upper inset), which allowed us to inject the current either parallel (x axis) or perpendicular (y axis) to the triangular base. The Nb films grown on the array of Ni triangles showed superconducting critical temperatures between 8.3 and 8.7 K.

Magneto-transport $R(H)$ experiments, R being the resistance, were done with a magnetic field H applied perpendicular to the substrate in a liquid helium system. Fig. 1B shows the $R(H)$ data taken from the sample

[1]Departamento de Física de Materiales, Facultad Ciencias Físicas, Universidad Complutense, 28040, Madrid, Spain. [2]Frontier Research System, The Institute of Physical and Chemical Research (RIKEN), Wako-shi, Saitama, 351–0198, Japan. [3]Center for Theoretical Physics, Department of Physics, University of Michigan, Ann Arbor, MI, 48109–1120, USA. [4]Instituto de Microelectrónica de Madrid, Centro Nacional Mícroelectrónica, Consejo Superior de Investigaciones Científicas, Isaac Newton 8, Tres Cantos, 28760 Madrid, Spain.

*To whom correspondence should be addressed. E-mail: jlvicent@fis.ucm.es